Supporting Information

Combined In-situ X-ray Spectroscopic and Theoretical Study on Trimetal Synergistic Enhancement of Water Oxidation

Yalei Fan, Xubin Ye, Jing Zhou, Dabiao Lu, Chang-yang Kuo, Yu-Cheng Huang, Ting-Shan Chan, Chien-Te Chen, Youwen Long, Jian-Qiang Wang*, Zhiwei Hu*, and Linjuan Zhang**

Y. Fan, J.-Q. Wang, L. Zhang
Key Laboratory of Interfacial Physics and Technology, Shanghai Institute of Applied Physics, Chinese Academy of Sciences, Shanghai 201800, P. R. China
University of Chinese Academy of Sciences, Beijing 100049, P. R. China
E-mail: wangjianqiang@sinap.ac.cn; zhanglinjuan@sinap.ac.cn.

X. Ye, D. Lu, Y. Long
Beijing National Laboratory for Condensed Matter Physics, Institute of Physics, Chinese Academy of Sciences, Beijing 100190, P. R. China
E-mail: ywlong@iphy.ac.cn

J. Zhou
Zhejiang Institute of Photoelectronics and Zhejiang Institute for Advanced Light Source, Zhejiang Normal University, Jinhua, Zhejiang 321004, P. R. China

C.-Y. Kuo, Y.-C. Huang, T.-S. Chan. C.-T. Chen
National Synchrotron Radiation Research Center, Hsinchu 30076, Taiwan, R. O. China

C.-Y. Kuo
Department of Electrophysics, National Yang Ming Chiao Tung University, Hsinchu 30010, Taiwan, R. O. China

Z. Hu
Max Planck Institute for Chemical Physics of Solids, Dresden 01187, Germany
E-mail: Zhiwei.Hu@cpfs.mpg.de

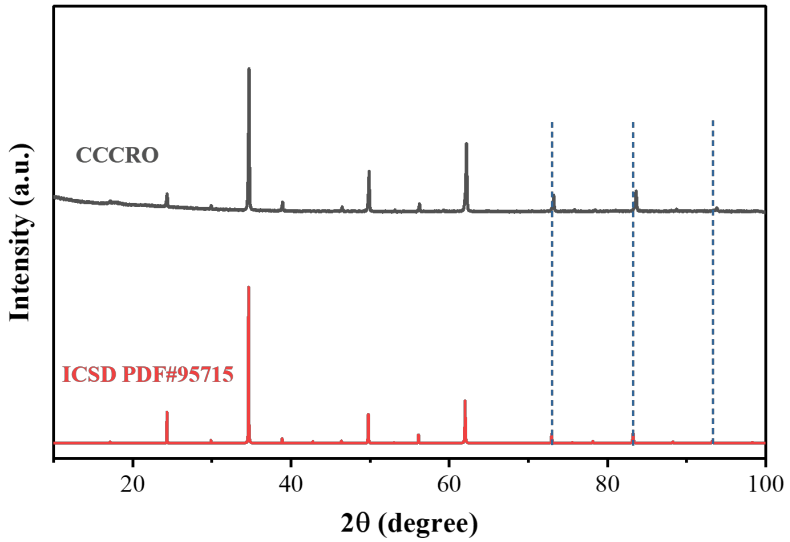

Figure S1. Lab-based XRD patterns of CCCRO powder.

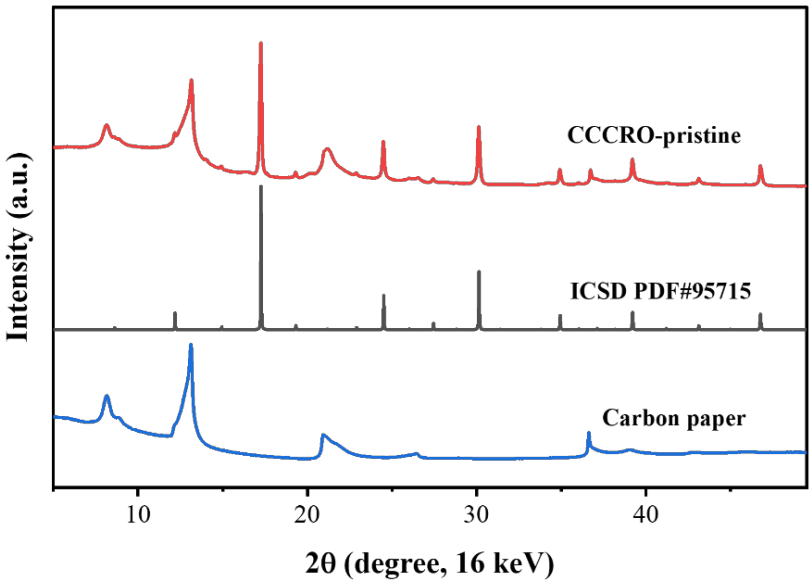

Figure S2. SR-based XRD pattern of CCCRO loaded on carbon paper.

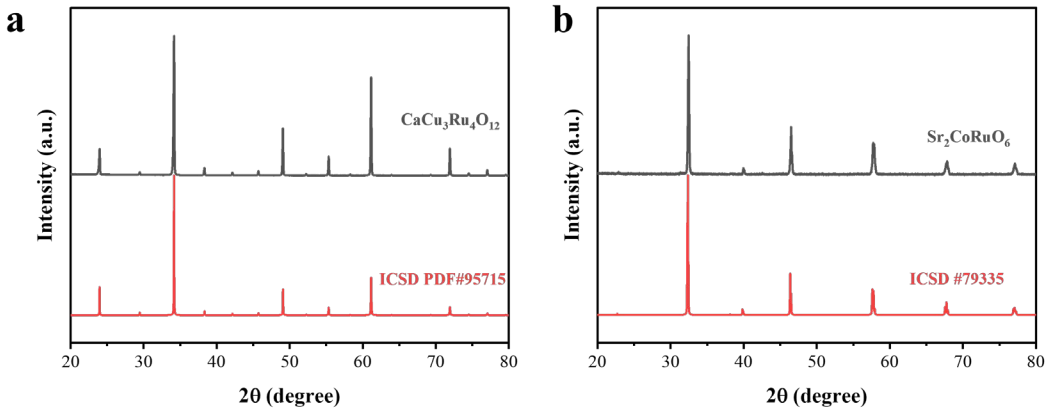

Figure S3. Lab-based XRD patterns of (a) $CaCu_3Ru_4O_{12}$, and (b) Sr_2CoRuO_6.

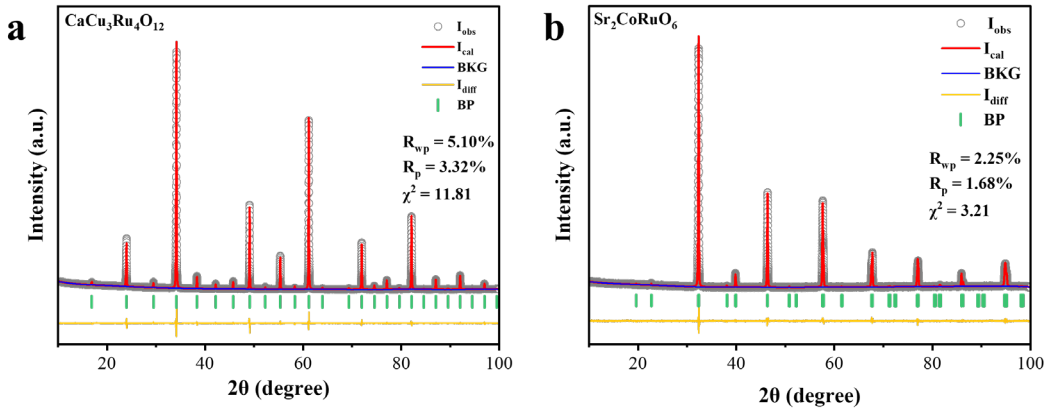

Figure S4. Refined XRD profiles of (a) $CaCu_3Ru_4O_{12}$, and (b) Sr_2CoRuO_6.

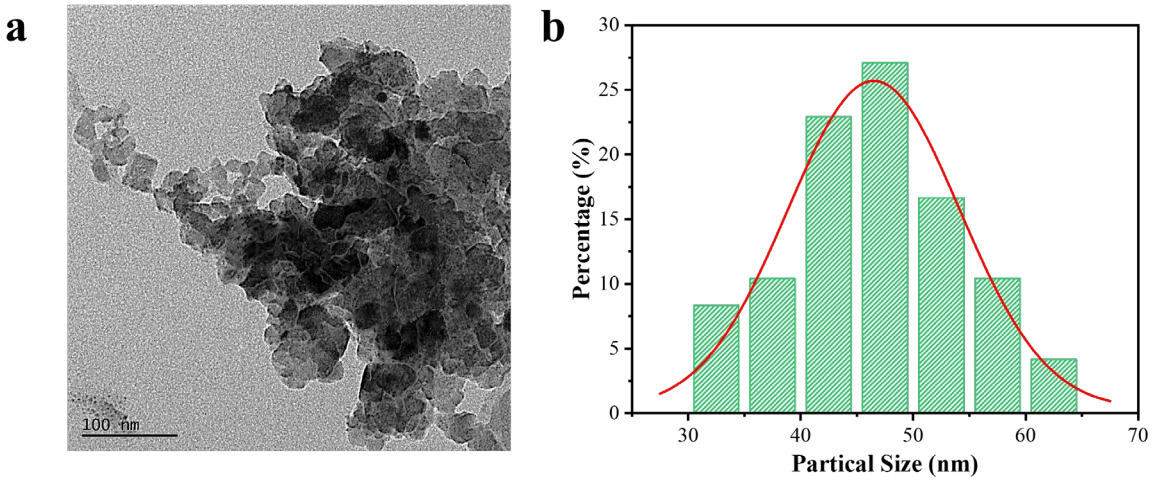

Figure S5. Particle size of CCCRO. (a) HRTEM images. (b) Particle size distribution determined using the diameters measured on the HRTEM image.

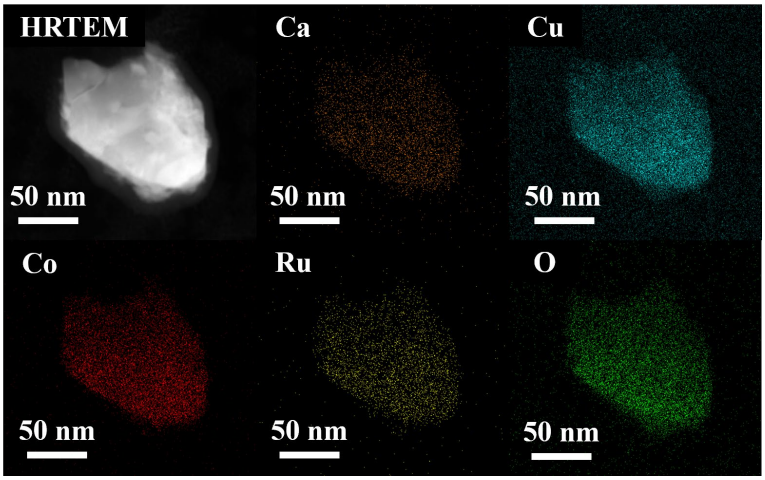

Figure S6. EDX elemental mapping for CCCRO.

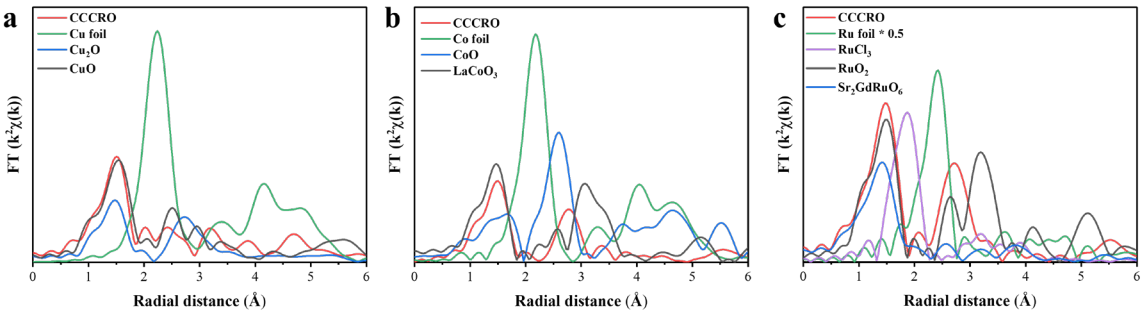

Figure S7. (a) Fourier transforms of k^2-weigted EXAFS spectra at Cu *K*-edge of CCCRO, Cu foil, Cu_2O and CuO. (b) Fourier transforms of k^2-weigted EXAFS spectra at Co *K*-edge of CCCRO, Co foil, CoO and $LaCoO_3$. (c) Fourier transforms of k^2-weigted EXAFS spectra at Ru *K*-edge of CCCRO, Ru foil, $RuCl_3$, RuO_2, and Sr_2GdRuO_6.

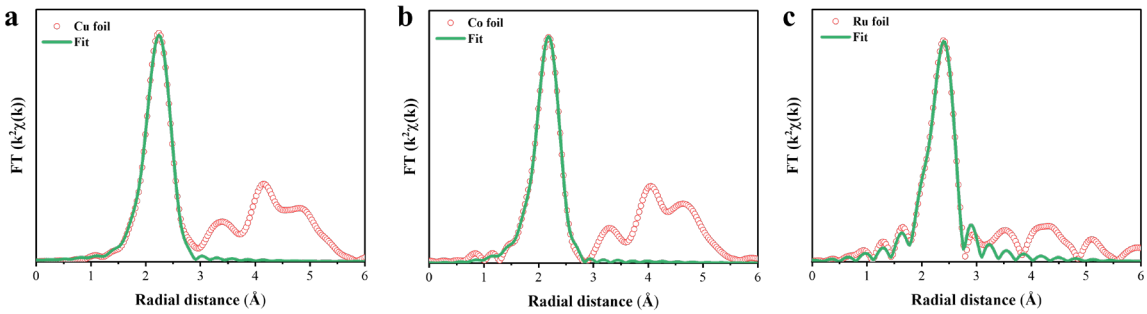

Figure S8. The EXAFS fitting curves for (a) Cu foil. (b) Co foil. (c) Ru foil.

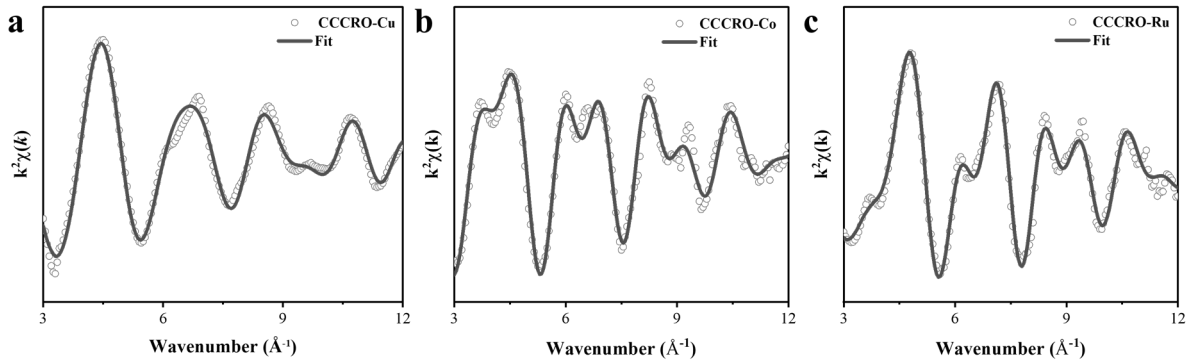

Figure S9. The EXAFS fitting curves of *K*-space for CCCRO.

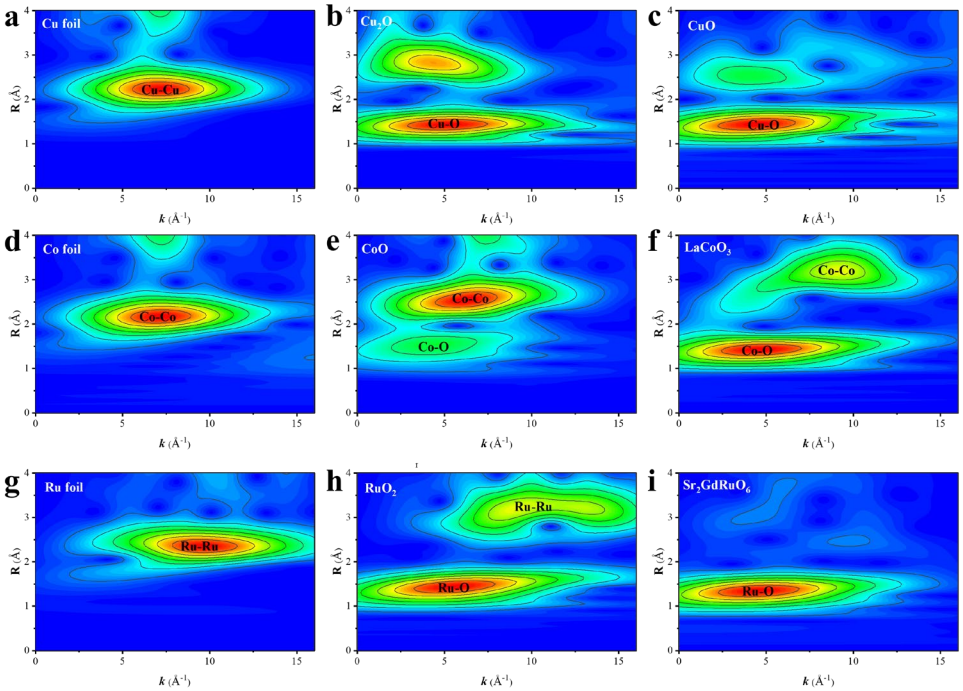

Figure S10. Wavelet transform for the k^2-weighted EXAFS spectra of (a) Cu foil, (b) Cu_2O, (c) CuO, (d) Co foil, (e) CoO, (f) $LaCoO_3$, (g) Ru foil, (h) RuO_2, and (i) Sr_2GdRuO_6.

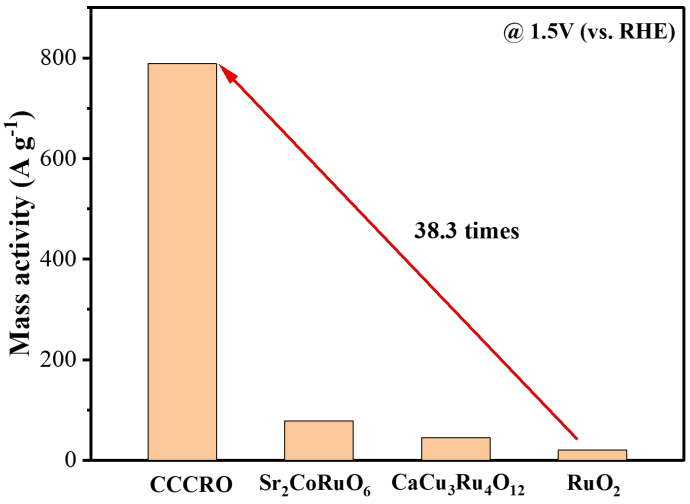

Figure S11. Mass activity of CCCRO, $CaCu_3Ru_4O_{12}$, Sr_2CoRuO_6, and RuO_2 were measured at 1.5 V.

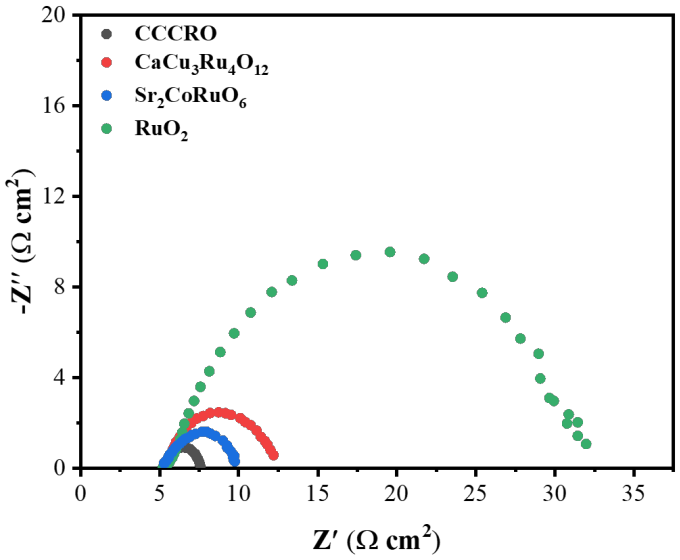

Figure S12. EIS of CCCRO, $CaCu_3Ru_4O_{12}$, Sr_2CoRuO_6, and RuO_2 were measured at 1.5 V.

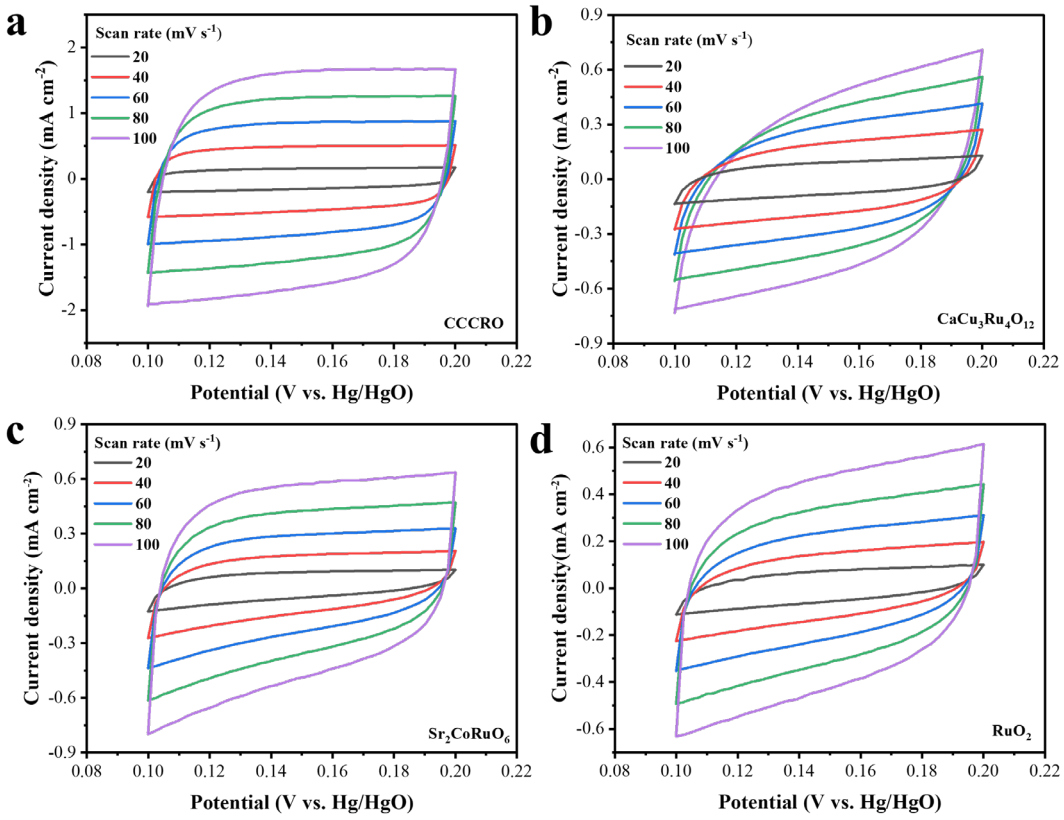

Figure S13. ECSA of (a) CCCRO, (b) $CaCu_3Ru_4O_{12}$, (c) Sr_2CoRuO_6, and (d) RuO_2.

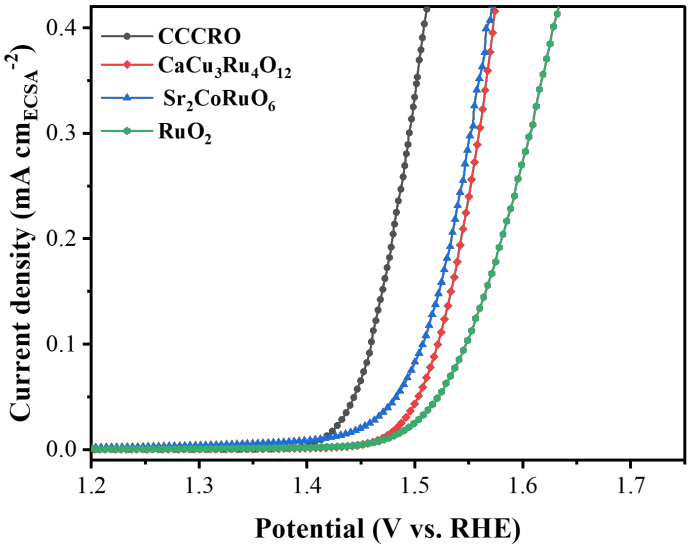

Figure S14. LSVs curves normalized by ECSA for CCCRO, $CaCu_3Ru_4O_{12}$, Sr_2CoRuO_6, and RuO_2.

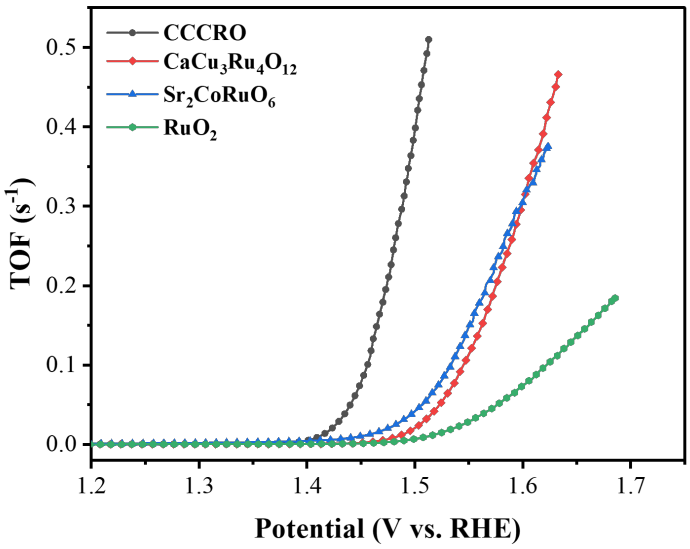

Figure S15. The plots of the TOFs value as a function of potential.

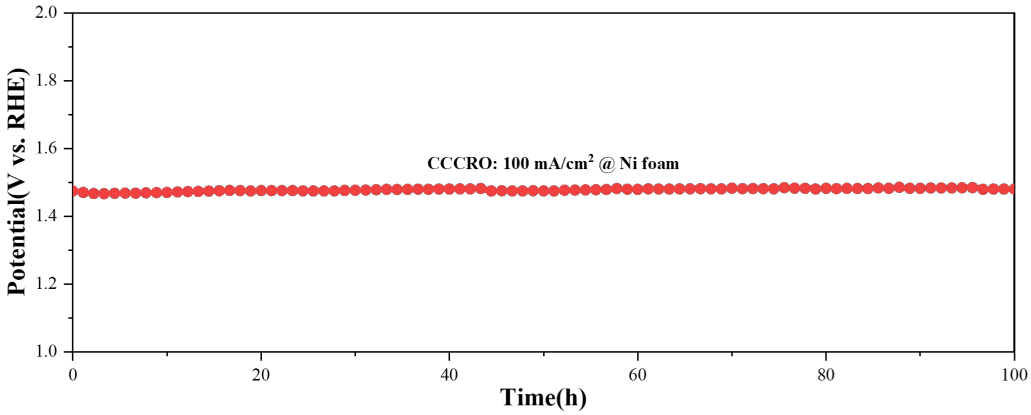

Figure S16. Long-term electrochemical stability of CCCRO was measured at the current density of 100 mA cm^{-2}.

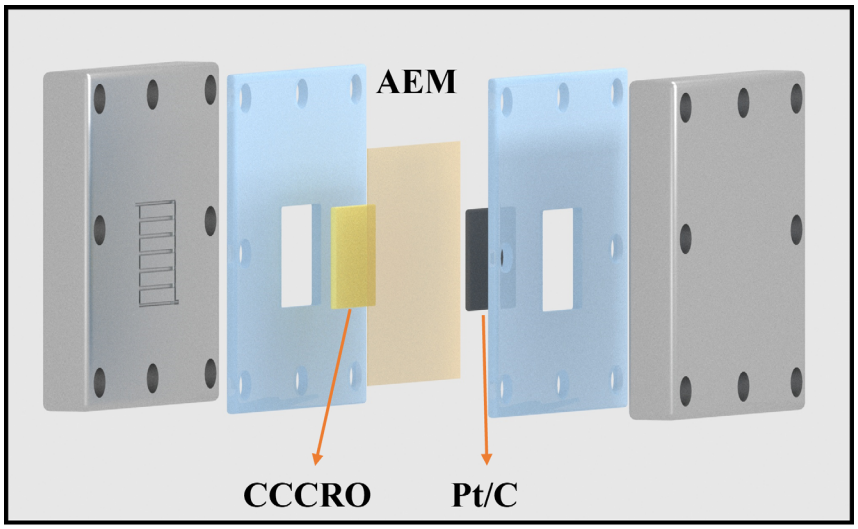

Figure S17. Schematic illustration of the AEM reactor.

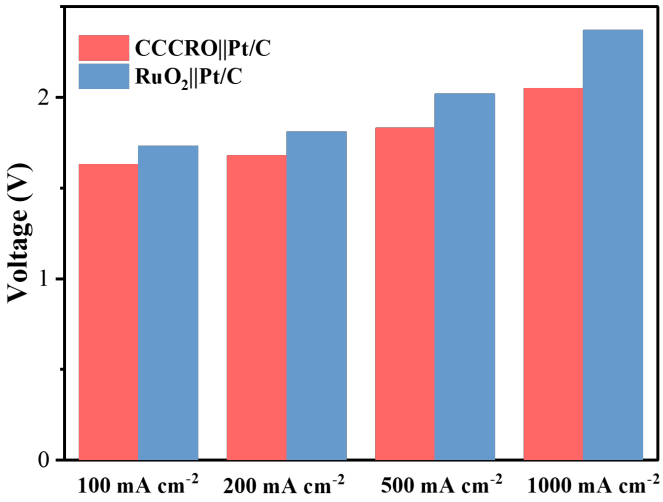

Figure S18. Cell voltage of the AEM electrolyzer at various current densities.

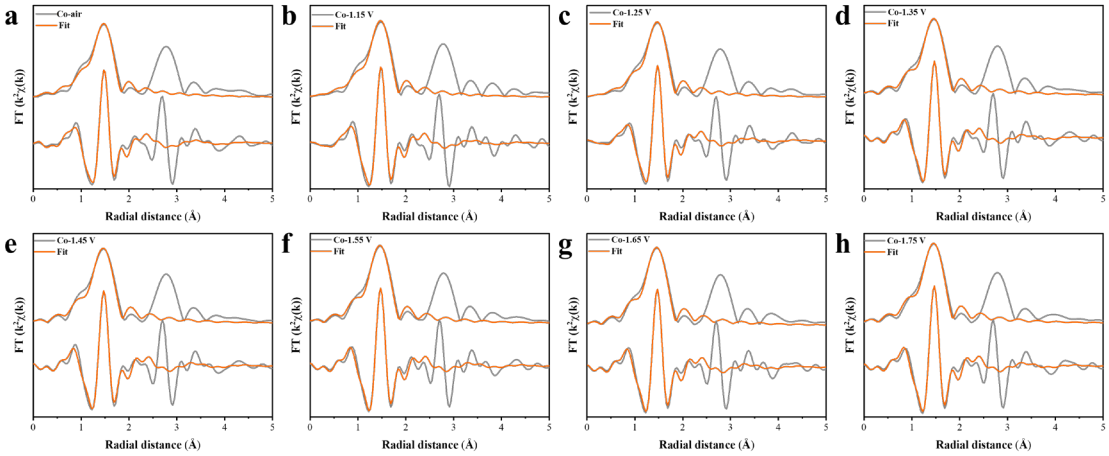

Figure S19. Fits for Co *K*-edge spectra of the CCCRO measured in KOH electrolyte (a) without and (b–h) with applied potentials. The Fourier transformation was carried out in over 3–12 Å $^{-1}$, and the fitting was carried out over 1–2 Å.

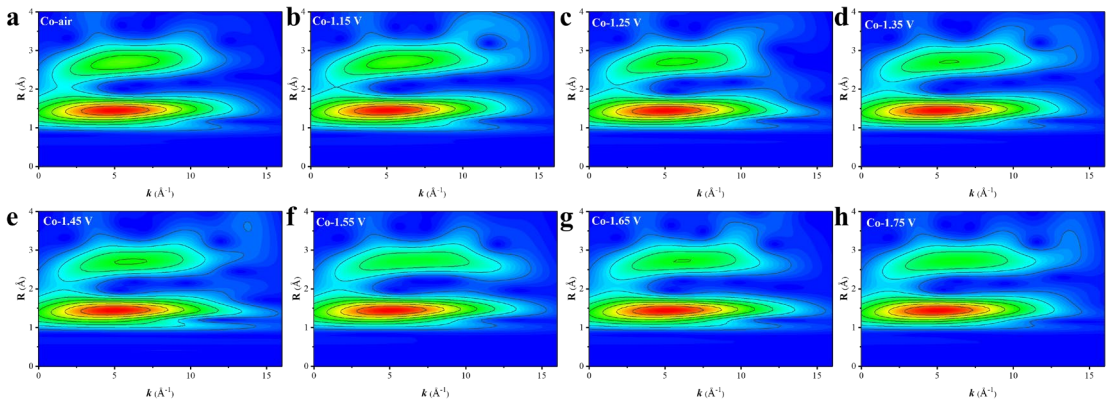

Figure S20. Wavelet transform for the k^2-weighted EXAFS spectra at Co *K*-edge of CCCRO (a) without and (b–h) with applied potentials.

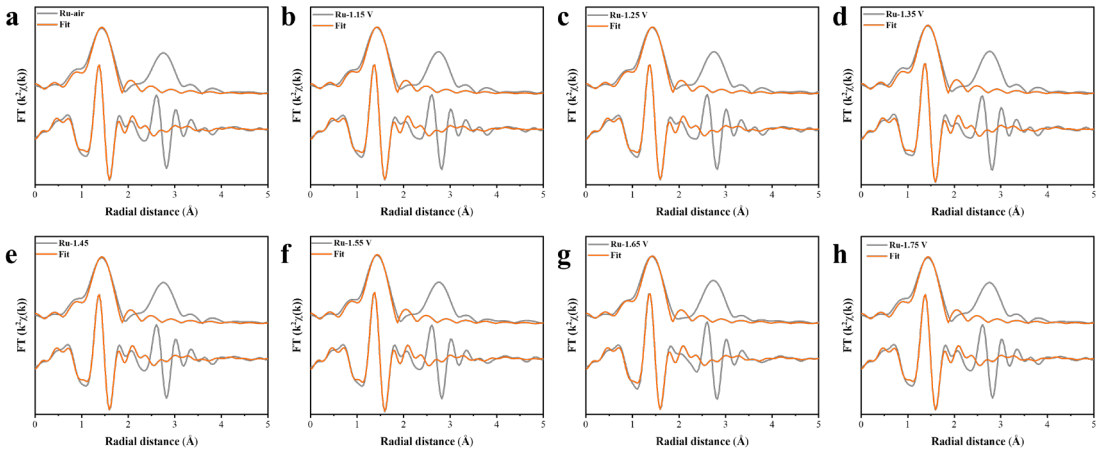

Figure S21. Fits for Ru *K*-edge spectra of the CCCRO measured in KOH electrolyte (a) without and (b–h) with applied potentials. The Fourier transformation was carried out in over 3–12 Å $^{-1}$, and the fitting was carried out over 1–2 Å.

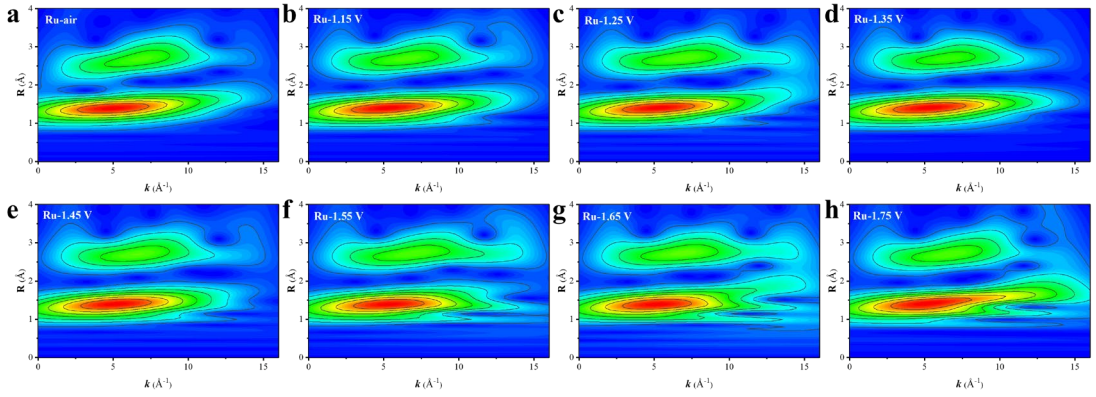

Figure S22. Wavelet transform for the k^2-weighted EXAFS spectra at Ru *K*-edge of CCCRO (a) without and (b–h) with applied potentials.

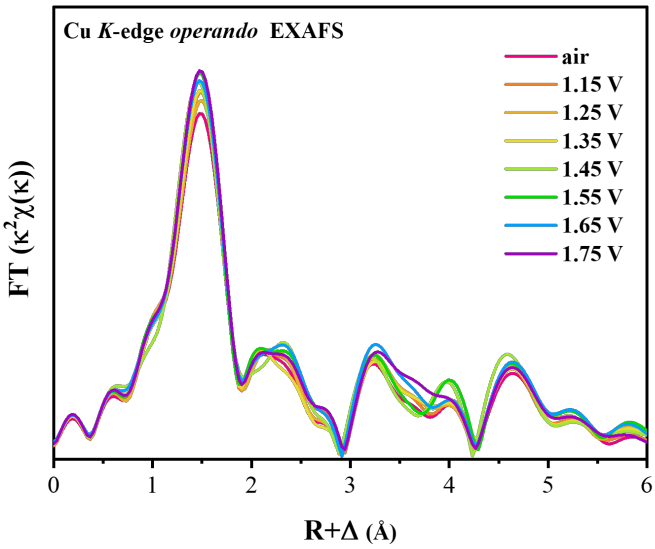

Figure S23. FT-EXAFS at the Cu *K*-edge.

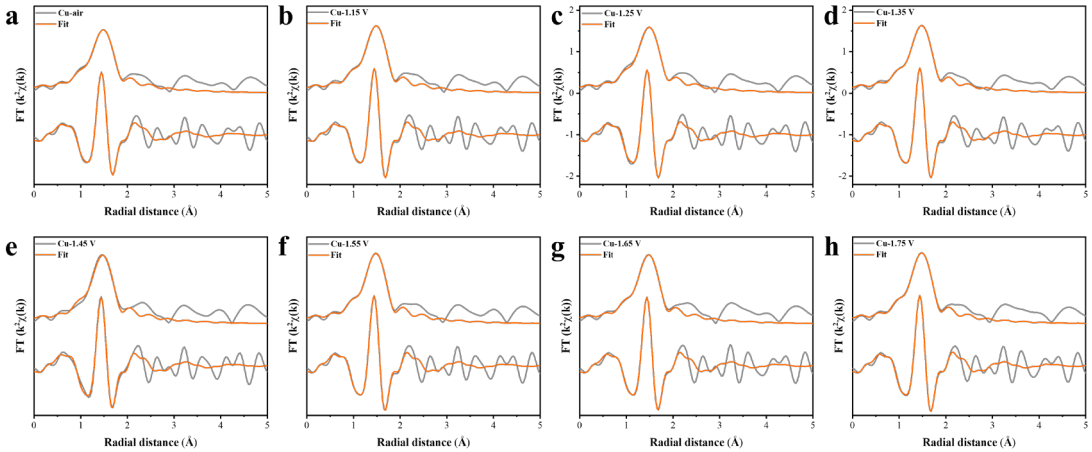

Figure S24. Fits for Cu *K*-edge spectra of the CCCRO measured in KOH electrolyte (a) without and (b–h) with applied potentials. The Fourier transformation was carried out in over 3–12 Å $^{-1}$, and the fitting was carried out over 1–2 Å.

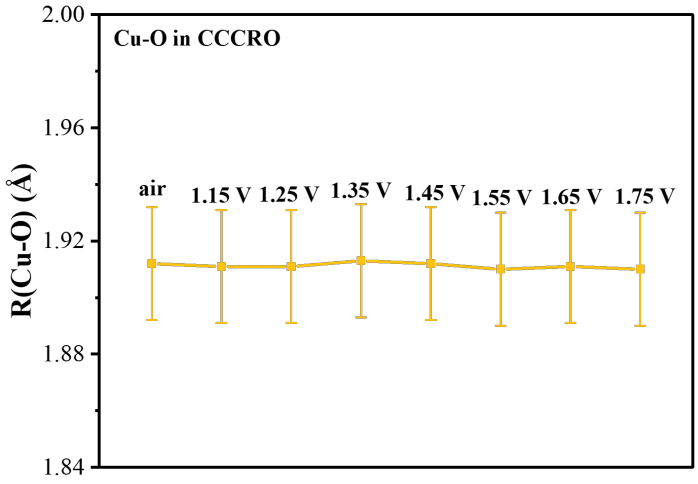

Figure S25. Cu-O bond length in CCCRO electrocatalyst under applied potential extracted from EXAFS fitting. The applied voltage is referenced to RHE.

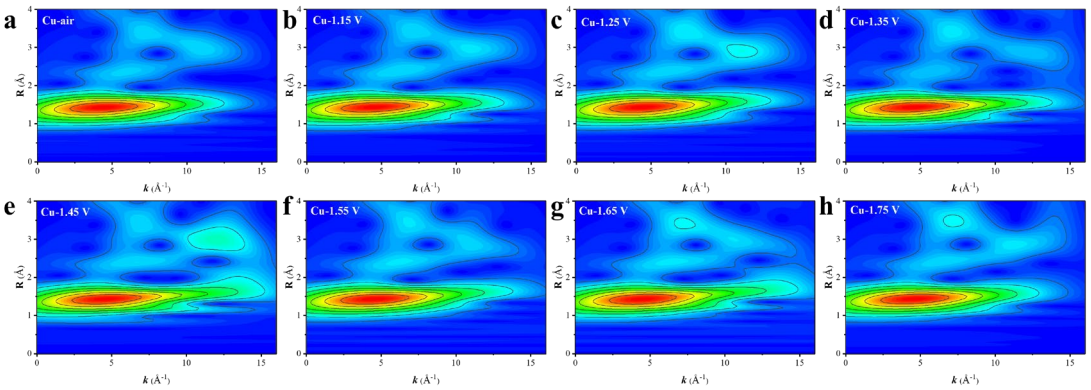

Figure S26. Wavelet transform for the k^2-weighted EXAFS spectra at Cu *K*-edge of CCCRO (a) without and (b–h) with applied potentials.

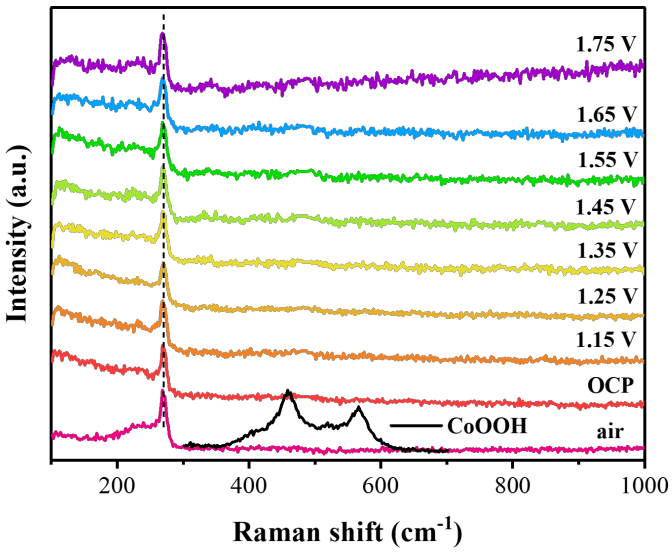

Figure S27. *In-situ* Raman spectroscopy of CCCRO.

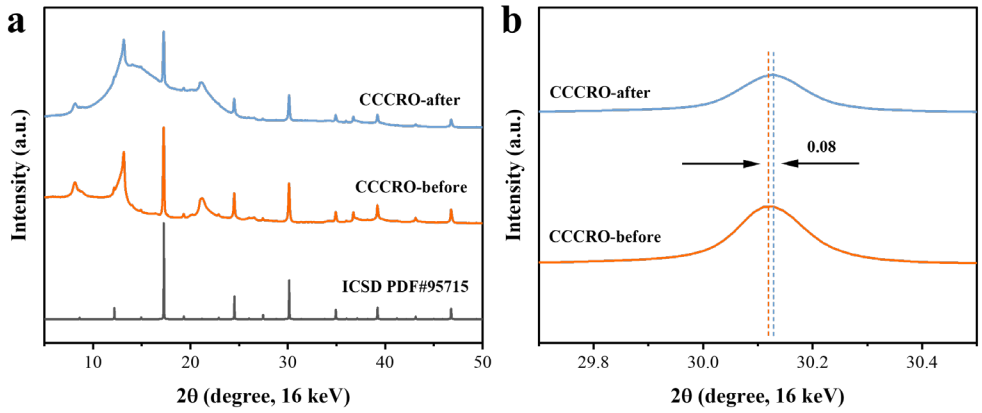

Figure S28. (a) and (b) SR-based XRD pattern of CCCRO loaded on carbon paper before and after the OER.

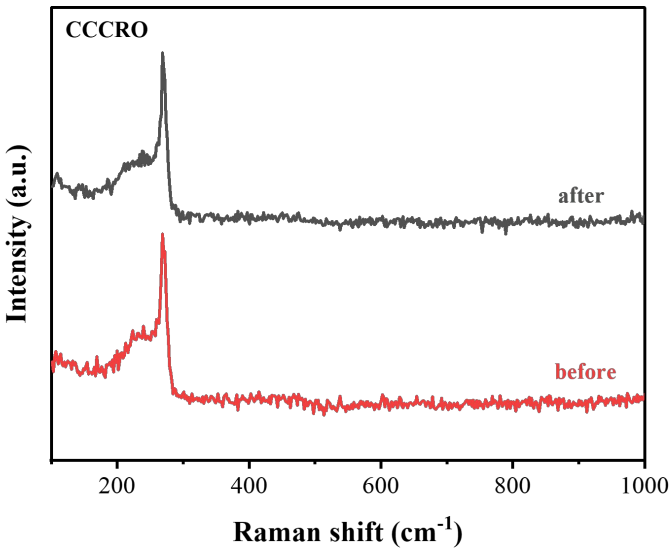

Figure S29. Raman spectroscopy of CCCRO before and after the OER.

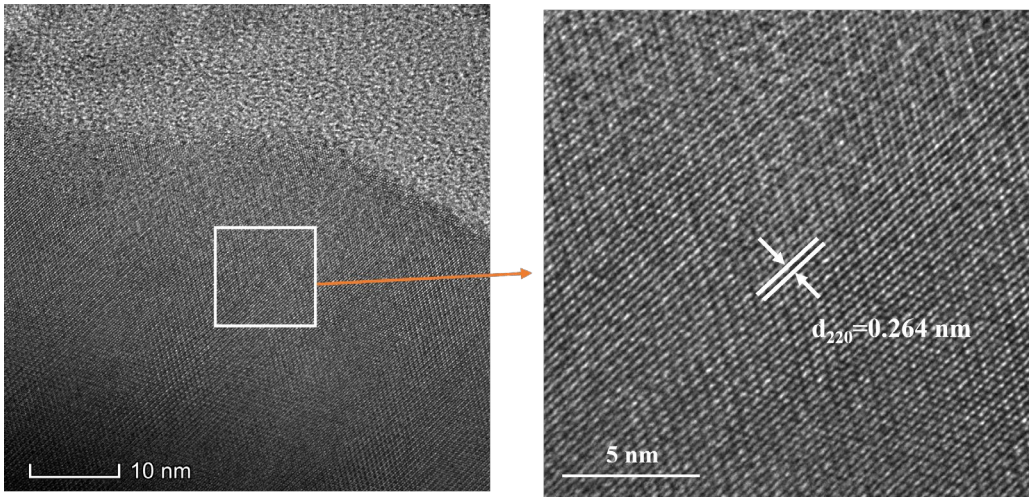

Figure S30. HRTEM images of CCCRO after the OER.

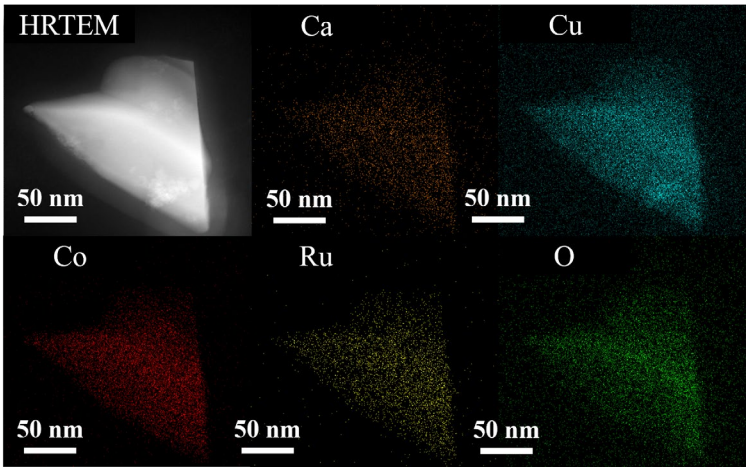

Figure S31. EDX images of CCCRO after the OER.

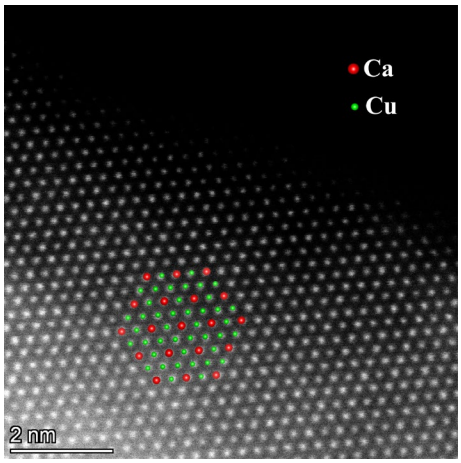

Figure S32. Atomic-resolution HAADF-STEM image of CCCRO after the OER. The red, green dots represent the Ca and Cu atoms, respectively.

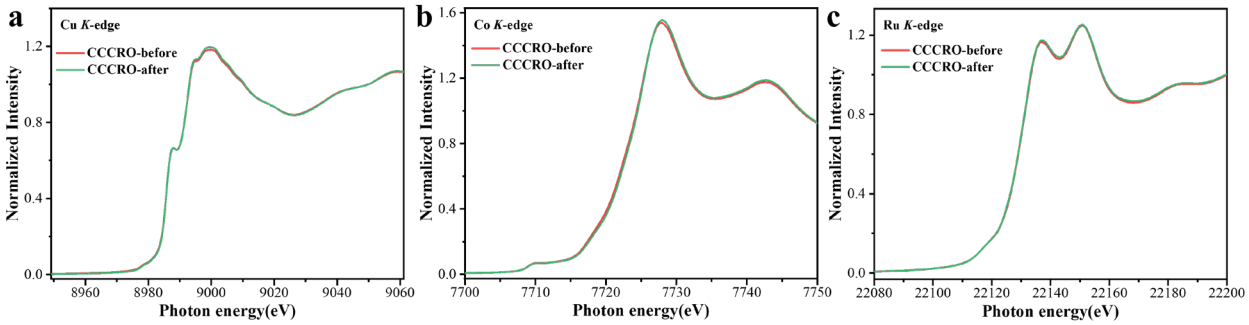

Figure S33. (a) Cu *K*-edge spectra of CCCRO after OER (green line) and before OER (red line). (b) Co *K*-edge spectra of CCCRO after OER (green line) and before OER (red line) (c) Ru *K*-edge spectra of CCCRO after OER (green line) and before OER (red line).

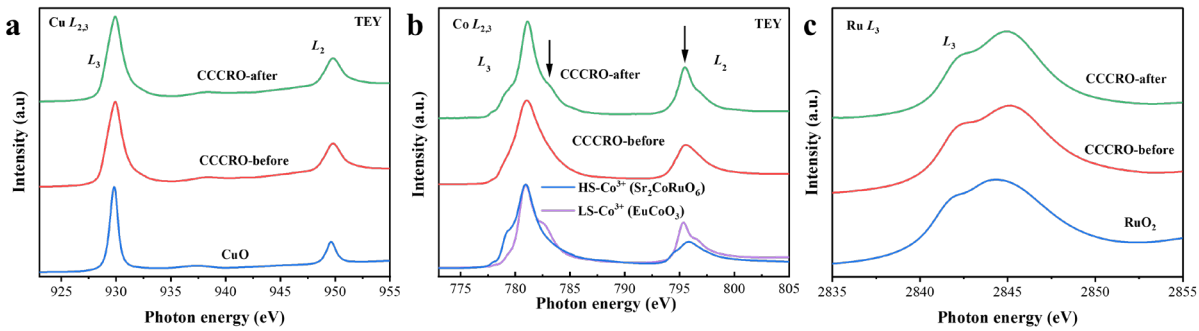

Figure S34. (a) Cu $L_{2,3}$-edge spectra of CCCRO after OER (green line), before OER (red line), and reference $Cu^{2+}O$ (blue line). (b) Co $L_{2,3}$-edge spectra of CCCRO after OER (green line), before OER (red line), and references HS-Co^{3+} ($Sr_2Co^{3+}RuO_6$, blue line) and LS-Co^{3+} ($EuCo^{3+}O_3$: pink line). (c) Ru L_3-edge spectra of CCCRO after OER (green line), before OER (red line), and reference $Ru^{4+}O_2$ (blue line).

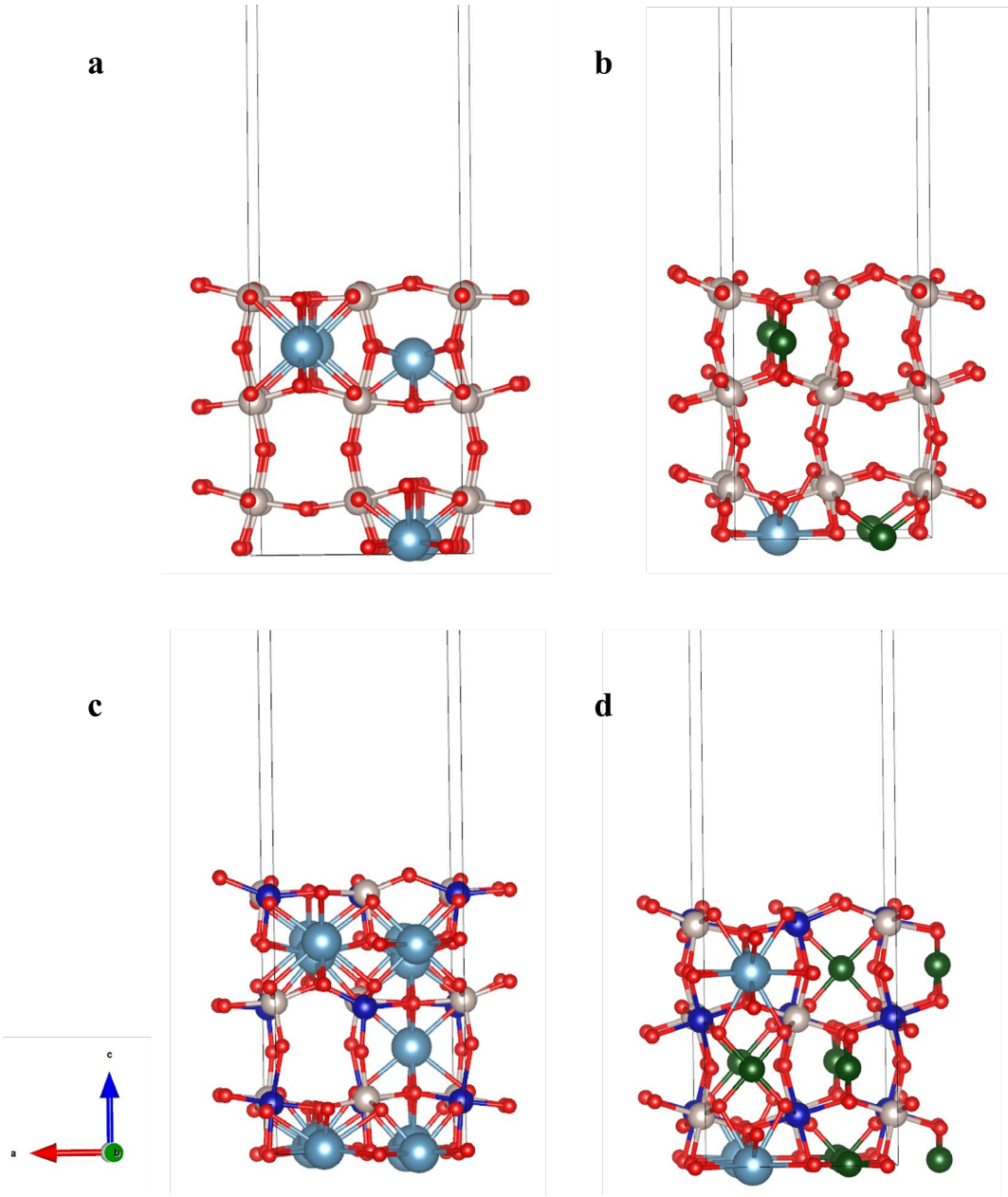

Figure S35. The optimized local structures for the (001) surface of (a) $Ca_{0.5}Ru_2O_6$, (b) $Ca_{0.5}Cu_{0.5}Ru_4O_{12}$, (c) $Ca_{1.5}CoRuO_6$, and (d) $Ca_{0.5}Cu_{2.5}Co_2Ru_2O_{12}$. The azure, green, blue, white, and red balls indicate Ca, Cu, Co, Ru, and O respectively.

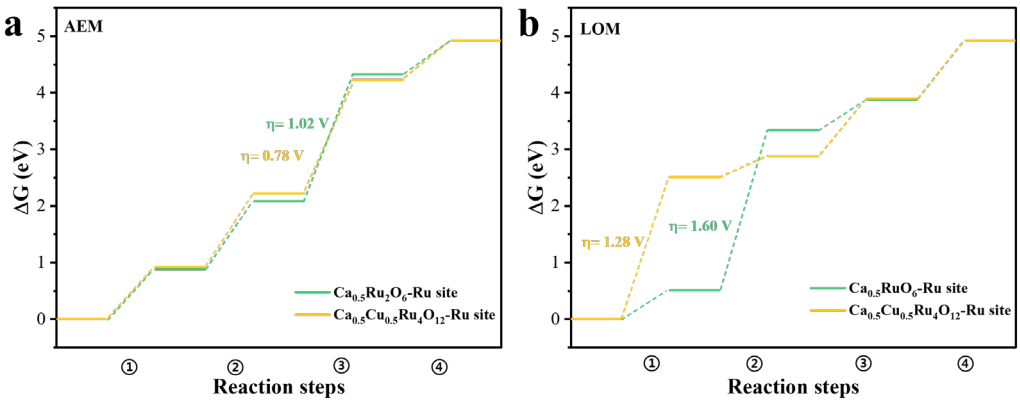

Figure S36. (a) AEM and, (b) LOM on $Ca_{0.5}Ru_2O_6$ and $Ca_{0.5}Cu_{0.5}Ru_4O_{12}$.

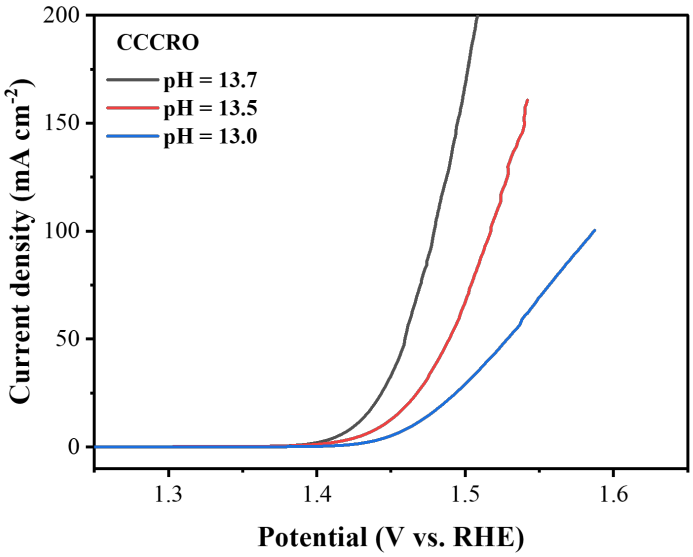

Figure S37. LSV curves of CCCRO in alkaline electrolytes with different pH values.

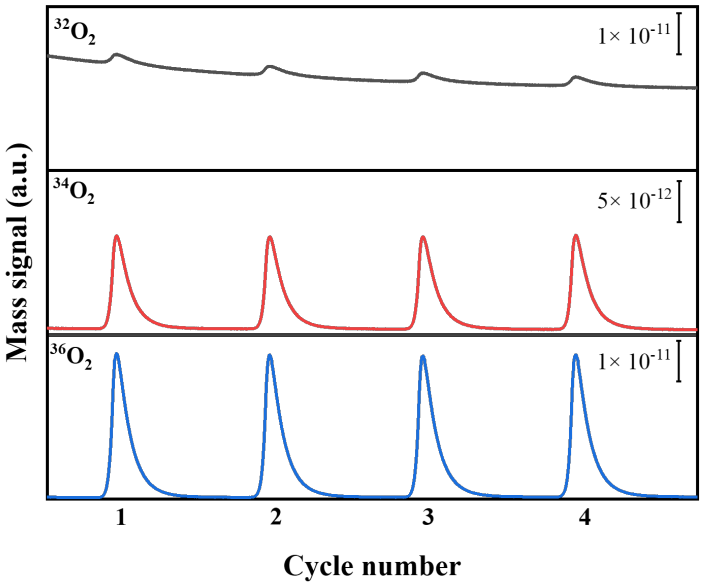

Figure S38. DEMS results were obtained for CCCRO with CV cycles in a $H_2{}^{18}O$-based 0.1M KOH electrolyte, within the potential range of 1.10–1.75 V (vs. RHE), using a can rate of 5 mV s^{-1}.

Table S1. Refined structural parameters of the as-prepared CCCRO.

Atom	*x*	*y*	*z*	Occupancy	U_{iso}
Ca1	0.00000	0.00000	0.00000	1.0000	0.0129
Cu1	0.00000	0.50000	0.50000	1.0000	0.0315
Ru1	0.25000	0.25000	0.25000	0.5175	0.0406
O1	0.34563(17)	0.13698(13)	0.00000	1.0000	0.0016
Co1	0.25000	0.25000	0.25000	0.4825	0.0406

Refined lattice parameters: *Im*-3 space group, a = b = c = 7. 30121(1) Å, α = β = γ = 90° and the unit cell volume V = 390.51 $Å^3$.

Table S2. The atomic percentage of each element in EDX (from HRTEM) of CCCRO.

Atom	Family	Atomic Fraction (%)	Atomic Error (%)
Ca	K	4.74	0.51
Cu	K	15.21	3.33
Co	K	9.85	2.16
Ru	K	11.17	2.64
O	K	59.03	3.71

Table S3. EXAFS fitting parameters for (a) Cu foil, Co foil, and Ru foil. (b) CCCRO.

(a) Cu foil, Co foil, and Ru foil.

Sample	Scattering path	*N*	*R* (Å)	$\sigma^2(10^{-3}Å^2)$	S_0^2	*R* factor
Cu foil	Cu-Cu	12*	2.542±0.01	8.7	0.86	0.003
Co foil	Co-Co	12*	2.491±0.06	6.5	0.81	0.008
Ru foil	Ru-Ru	6*	2.618±0.03	3.1	0.65	0.007
	Ru-Ru	6*	2.734±0.02	3.3		

(b) CCCRO.

Sample	Scattering path	*N*	*R* (Å)	σ^2(10^{-3}Å^2)	*R* factor
CCRO-Cu	Cu-O	4.0±0.3	1.912±0.01	3.4	0.005
	Co-O	5.9±0.4	1.933±0.02	4.2	
CCRO-Co	Co-Ca	2.5±1.2	3.142±0.01	6.8	0.006
	Co-Cu	6.0±0.8	3.213±0.05	8.3	
	Ru-O	5.9±0.5	1.972±0.01	3.6	
CCRO-Ru	Ru-Ca	2.3±1.1	3.072±0.01	9.2	0.004
	Ru-Cu	6.2±1.3	3.114±0.03	7.7	

The EXAFS oscillations were extracted from the normalized XAS spectra by subtracting the atomic background using a cubic spline fit to k^2-weighted data, where k is the photoelectron wave number. The χ(k) functions were the Fourier transformed into R-space. The Fourier-transform window was in the k range 3–12 Å^{-1}. *CN*, coordination number; *R*, distance between absorber and backscatter atoms; σ^2, Debye-Waller factor to account for both thermal and structural disorders; *R* factor indicates the goodness of the fit. S_0^2 was fixed to 0.86/0.81/0.65, according to the experimental EXAFS fit of Cu/Co/Ru foil by fixing CN as the known crystallographic value.

Table S4. Comparison of OER performance with previous reported high activity Co-Ru based OER catalysts.

No.	Catalyst	η_{10} (mV)	Electrolyte	Reference
1	CCCRO	198	1 M KOH	This work
2	Co-SAC/RuO_2	200	1 M KOH	[1]
3	(SA-Ru/Co(OH)F)	200	1 M KOH	[2]
4	$RuCoO_x$/NC-350	210	1 M KOH	[3]
5	RuO_2/Co_3O_4–RuCo-EO	220	1 M KOH	[4]
6	Co-$ZnRuO_x$	224	1 M KOH	[5]
7	Co-Ru-Py@500	230	1 M KOH	[6]
8	2% Ru-NCO	233	1 M KOH	[7]
9	CoRu-O/A@HNC-2	234	1 M KOH	[8]
10	VCo-RCO	240	1 M KOH	[9]
11	Ru/Co-N-C	247	1 M KOH	[10]
12	Ru-Co/ELCO	247	1 M KOH	[11]
13	IW-Co_3O_4-RuO_2-HS	250	1 M KOH	[12]
14	Sr_2CoRuO_6	254	1 M KOH	This work
15	Co-Ni-Ru-S-Se	261	1 M KOH	[13]
16	(Ru-Co)O_x-350	265	1 M KOH	[14]
17	Ru/Co_3O_{4-x}	280	1 M KOH	[15]
18	Ru/Ni-Co_3O_4	290	1 M KOH	[16]
19	Ru-Co_3O_4-15	292	1 M KOH	[17]
20	Ru-Co_3O_4/CoP/TM Ru	293	1 M KOH	[18]
21	RuO_2/Co_3O_4	302	1 M KOH	[19]
22	CoO/$Ru_{1.25\%}$HPNs	308	1 M KOH	[20]
23	Co-Ru-MoS_2	308	1 M KOH	[21]
24	Co/Ru SAs-N-C	338	1 M KOH	[22]
25	$RuCoO_x$@Co/N-CNT	350	1 M KOH	[23]

Table S5. EXAFS fitting parameters for Co *K*-edge under potentials.

Sample	Scattering path	*N*	*R* (Å)	σ^2(10^{-3}Å^2)	*R* factor
Co air	Co-O	5.9±0.3	1.934±0.02	3.7	0.007
Co 1.15 V	Co-O	5.9±0.5	1.926±0.01	3.4	0.011
Co 1.25 V	Co-O	5.8±0.6	1.914±0.02	4.5	0.010
Co 1.35 V	Co-O	5.7±1.1	1.912±0.02	4.3	0.008
Co 1.45 V	Co-O	5.8±1.5	1.911±0.02	5.6	0.012
Co 1.55 V	Co-O	5.7±1.7	1.908±0.02	5.3	0.007
Co 1.65 V	Co-O	5.6±1.6	1.901±0.02	6.7	0.009
Co 1.75 V	Co-O	5.6±1.5	1.897±0.02	8.9	0.008

Table S6. EXAFS fitting parameters for Ru *K*-edge under potentials.

Sample	Scattering path	*N*	*R* (Å)	σ^2(10^{-3}Å^2)	*R* factor
Ru air	Ru-O	5.9±0.6	1.972±0.01	4.3	0.008
Ru 1.15 V	Ru -O	6.1±1.2	1.963±0.02	3.2	0.013
Ru 1.25 V	Ru -O	6.0±0.8	1.957±0.02	5.3	0.011
Ru 1.35 V	Ru -O	5.9±1.4	1.946±0.02	4.0	0.014
Ru 1.45 V	Ru-O	5.8±2.1	1.934±0.02	6.6	0.014
Ru 1.55 V	Ru-O	5.8±1.9	1.932±0.02	5.8	0.013
Ru 1.65 V	Ru-O	5.7±1.5	1.927±0.02	7.3	0.015
Ru 1.75 V	Ru-O	5.7±1.7	1.925±0.02	6.6	0.014

Table S7. EXAFS fitting parameters for Cu *K*-edge under potentials.

Sample	Scattering path	*N*	*R* (Å)	$\sigma^2(10^{-3}Å^2)$	*R* factor
Cu air	Cu-O	4.1±0.2	1.912±0.02	4.4	0.003
Cu 1.15 V	Cu -O	4.0±0.2	1.911±0.02	3.5	0.004
Cu 1.25 V	Cu -O	4.2±0.4	1.911±0.02	4.1	0.005
Cu 1.35 V	Cu -O	4.0±0.2	1.913±0.02	3.6	0.003
Cu 1.45 V	Cu-O	4.2±0.5	1.912±0.02	3.8	0.005
Cu 1.55 V	Cu-O	4.2±0.7	1.910±0.02	3.3	0.008
Cu 1.65 V	Cu-O	4.3±1.1	1.911±0.02	3.9	0.007
Cu 1.75 V	Cu-O	4.1±0.6	1.910±0.02	3.4	0.006

Table S8. The atomic percentage of each element in EDX (from HRTEM) of CCCRO after the OER.

Atom	Family	Atomic Fraction (%)	Atomic Error (%)
Ca	K	3.17	2.31
Cu	K	14.35	2.74
Co	K	10.83	3.37
Ru	K	12.18	3.15
O	K	59.74	6.72

Table S9. The atomic percentage of different elements in the CCCRO before and after the OER (at 100 mA cm^{-2} for 50 h) measured by ICP-MS.

CCCRO	Ca%	Cu%	Co%	Ru%
before	12.42	37.64	24.85	25.09
after	7.56	35.43	28.02	28.99

Table S10. The computed Gibbs free energy change and overpotentials (η) for the $Ca_{0.5}Ru_2O_6$, $Ca_{0.5}Cu_{0.5}Ru_4O_{12}$, $Ca_{1.5}CoRuO_6$, and $Ca_{0.5}Cu_{2.5}Co_2Ru_2O_{12}$ in the (a) AEM, and (b) LOM. mechanism.

(a) AEM

catalyst	step ①	step ②	step ③	step ④	η (V)
$Ca_{0.5}Ru_2O_6$-Ru site	0.88	1.20	2.25	1.19	1.02
$Ca_{0.5}Cu_{0.5}Ru_4O_{12}$-Ru site	0.92	1.30	2.01	0.69	0.78
$Ca_{1.5}CoRuO_6$-Co site	1.29	2.16	0.18	1.29	0.93
$Ca_{1.5}CoRuO_6$-Ru site	1.22	2.10	0.17	1.43	0.87
$Ca_{0.5}Cu_{2.5}Co_2Ru_2O_{12}$-Co site	1.28	2.00	0.99	0.65	0.77
$Ca_{0.5}Cu_{2.5}Co_2Ru_2O_{12}$-Ru site	1.35	0.91	1.91	0.75	0.68

(b) LOM

catalyst	step ①	step ②	step ③	step ④	η (V)
$Ca_{0.5}Ru_2O_6$-Ru site	0.51	2.83	0.54	1.04	1.60
$Ca_{0.5}Cu_{0.5}Ru_4O_{12}$-Ru site	2.51	0.37	1.02	1.02	1.28
$Ca_{1.5}CoRuO_6$-Co site	1.25	1.07	1.98	0.62	0.75
$Ca_{1.5}CoRuO_6$-Ru site	1.07	1.80	0.95	1.10	0.57
$Ca_{0.5}Cu_{2.5}Co_2Ru_2O_{12}$-Co site	1.54	0.47	1.55	1.36	0.32
$Ca_{0.5}Cu_{2.5}Co_2Ru_2O_{12}$-Ru site	1.61	0.54	1.37	1.40	0.38

References

[1] K. Shah, R. Dai, M. Mateen, Z. Hassan, Z. Zhuang, C. Liu, M. Israr, W.-C. Cheong, B. Hu, R. Tu, C. Zhang, X. Chen, Q. Peng, C. Chen, Y. Li, *Angew. Chem. Int. Ed*. **2022**, 61, e202114951.

[2] S. Zhou, H. Jang, Q. Qin, Z. Li, M. G. Kim, C. Li, X. Liu, J. Cho, *Sci. China Mater.* **2021**, 64, 1408–1417.

[3] Y. Tuo, W. Liu, C. Chen, Q. Lu, Y. Zhou, J. Zhang, *Chem. Asian J.* **2021**, 16, 2511.

[4] L. Tan, A. Zhang, Z. Liu, P. Yang, H. Guo, H. Fang, J. Han, Y. Zhu, Z. Ren, *RSC Adv.* **2021**, 11, 11779.

[5] D. Liu, Z. Wu, J. Liu, H. Gu, Y. Li, X. Li, S. Liu, S. Liu, J. Zhang, *Small* **2023**, 19, 2207235.

[6] L. Zeng, G. Mao, Y. Zhu, R. Li, Q. Zhou, F. Xiao, R. Tang, *Appl. Surf. Sci.* **2022**, 589,

152958.

[7] J. Zhang, J. Lian, Q. Jiang, G. Wang, *Chem. Eng. J* **2022**, 439, 135634.

[8] G. Li, K. Zheng, W. Li, Y. He, C. Xu, *ACS Appl. Mater. Interfaces* **2020**, 12, 51437.

[9] S. Pan, L. Zhang, M. Liu, X. Pan, M. Bi, T. Guo, Y. Zhang, J. Sun, A. Vasiliev, X. Ouyang, X. Wang, J. Zhu, Y. Fu, *ACS Sustain. Chem. Eng.* **2022**, 11, 290.

[10] C. Rong, X. Shen, Y. Wang, L. Thomsen, T. Zhao, Y. Li, X. Lu, R. Amal, C. Zhao, *Adv. Mater.* **2022**, 34, 2110103.

[11] X. Zheng, J. Yang, Z. Xu, Q. Wang, J. Wu, E. Zhang, S. Dou, W. Sun, D. Wang, Y. Li, *Angew. Chem. Int. Ed.* **2022**, 61, e202205946.

[12] Y. Gao, D. Zheng, Q. Li, W. Xiao, T. Ma, Y. Fu, Z. Wu, L. Wang, *Adv. Funct. Mater.* **2022**, 32, 2203206.

[13] W. Deng, W. Xie, D. Li, Y. Gai, Z. Chen, J. Yu, R. Yang, X. Bao, F. Jiang, *NPG Asia Mater.* **2022**, 14, 25.

[14] C. Wang, H. Shang, J. Li, Y. Wang, H. Xu, C. Wang, J. Guo, Y. Du, *Chem. Eng. J.* **2021**, 420, 129805.

[15] C.-Z. Yuan, S. Wang, K. San Hui, K. Wang, J. Li, H. Gao, C. Zha, X. Zhang, D. A. Dinh, X.-L. Wu, Z. Tang, J. Wan, Z. Shao, K. N. Hui, *ACS Catal.* **2023**, 13, 2462.

[16] B. Guo, R. Ma, Z. Li, J. Luo, M. Yang, J. Wang, *Mater. Chem. Front.* **2020**, 4, 1390.

[17] R. Madhu, A. Karmakar, P. Arunachalam, J. Muthukumar, P. Gudlur, S. Kundu, *J. Mater. Chem. A* **2023**, 11, 21767.

[18] K. Zhang, W. Ma, G. Tan, Z. Cheng, Y. Ma, W. Li, X. Feng, Z. Li, *Mol. Catal.* **2022**, 530, 112640.

[19] B.-Y. Guo, X.-Y. Zhang, X. Ma, T.-S. Chen, Y. Chen, M.-L. Wen, J.-F. Qin, J. Nan, Y.-M. Chai, B. Dong, *Int. J. Hydrogen Energy* **2020**, 45, 9575.

[20] D. Guo, C. Chen, Y. Wang, Y. Wang, C. Zhang, *J. Mater. Chem. C* **2023**, 11, 6336.

[21] I. S. Kwon, T. T. Debela, I. H. Kwak, Y. C. Park, J. Seo, J. Y. Shim, S. J. Yoo, J. G. Kim, J. Park, H. S. Kang, *Small* **2020**, 16, 2000081.

[22] L. Zhang, J. Yao, J. Zhang, W. He, Y. Li, L. Liang, C. Liu, H. Liu, Q. Hao, *Catal. Sci. Technol.* **2022**, 12, 5435.

[23] J. Yang, L. Chang, H. Guo, J. Sun, J. Xu, F. Xiang, Y. Zhang, Z. Wang, L. Wang, F. Hao, X. Niu, *J. Mater. Chem. A* **2020**, 8, 1229.